University of South Florida

Digital Commons @ University of South Florida

Anthropology Faculty Publications   Anthropology

2019

Geological Sources of Obsidian on Lipari and Artifact Production and Distribution in the Neolithic and Bronze Age Central Mediterranean

Robert Tykot
University of South Florida, rtykot@usf.edu

Follow this and additional works at: https://digitalcommons.usf.edu/ant_facpub

Original Study

Robert H. Tykot*

Geological Sources of Obsidian on Lipari and Artifact Production and Distribution in the Neolithic and Bronze Age Central Mediterranean

Abstract: The Aeolian island of Lipari, just north of eastern Sicily, was a major geological source of high quality obsidian that was volcanically formed in the Late Mesolithic, followed by another major production in the 1st millennium AD. A much earlier volcanic event on Lipari also produced some obsidian, but not of sufficient quality for tool production. A detailed geological survey of the Lipari obsidian source areas, including assessments of quantity, quality, accessibility, and visual variation was performed, followed by elemental analyses using INAA, LA-ICP-MS, ED-XRF, and pXRF which show that many different groups may be distinguished from each other. Geochemical analyses of several thousand obsidian artifacts from sites in Sicily and southern Italy reveal that two early Holocene subsources, Gabellotto Gorge and Canneto Dentro, were used during the Neolithic and Bronze Ages.

1 Introduction

The purpose of this study was to broaden our knowledge of the prehistoric Lipari obsidian trade network by chemically analyzing specific geological outcrops and distinguishing subsources of Lipari obsidian in order to identify and address potentially different material quality and quantity, accessibility, territorial control, and tool production and distribution in the central Mediterranean. Obsidian is a volcanic glass that was commonly used in the production of stone tools during the Neolithic and Bronze Age periods (ca. 6000–1000 BC) in the central Mediterranean. Workable quality obsidian that was available in prehistory has been identified as coming from four volcanic islands off the western and southern coasts of Italy: Sardinia, Palmarola, Pantelleria, and Lipari. Obsidian can be chemically characterized by a variety of analytical methods, including instrumental neutron activation analysis (INAA), laser ablation ICP mass spectrometry (LA-ICP-MS), and portable X-ray fluorescence (pXRF), which allows researchers to differentiate most if not all geological sources. The identification of the source of obsidian artifacts allows archaeologists to reconstruct prehistoric trade networks and patterns of socioeconomical interaction by tracing the distribution of obsidian from community to community over time and space.

*Corresponding author: Robert H. Tykot, University of South Florida, Tampa, FL 33556, USA, E-mail: rtykot@usf.edu

2 Geological Background

Lipari is one of seven volcanic islands in the Aeolian Archipelago (also Alicudi, Filicudi, Panarea, Salina, Stromboli, Vulcano), off the northeastern coast of Sicily and not far from the straits of Messina (Figure 1). These islands span a distance of about 75 km east-west, and 50 km north-south, while Lipari is located in the southeast quadrant, 30 km from Sicily. At 37.6 km², Lipari is also the largest of the Aeolian islands. Lipari was the second of these islands to be formed by subaerial volcanic activity (ca. 267–256 ka), and the first to produce any obsidian, on its southern end with the Monte Guardia eruptions dated ca. 27–24 cal ka (Forni et al., 2013, p. 245). Survey conducted in this area by the author, however, has not found any geological samples sufficiently large enough to produce stone tools (Tykot et al., 2006). In the early Holocene, however, high quality obsidian outcrops were formed in the Vallone del Gabellotto-Monte Pilato in eastern Lipari. Early fission track dating studies of obsidian artifacts had already indicated the rather late geological formation time for Lipari-Gabellotto, which was the most recent of all of the Mediterranean obsidian sources (Arias-Radi et al., 1972; Arias et al., 1984; Bigazzi & Bonadonna, 1973; Keller, 1970; Wagner et al., 1976), but the precision of such measurements, which range over at least a few thousand years, is insufficient to address the specific cultural time frame when Lipari obsidian first became available.
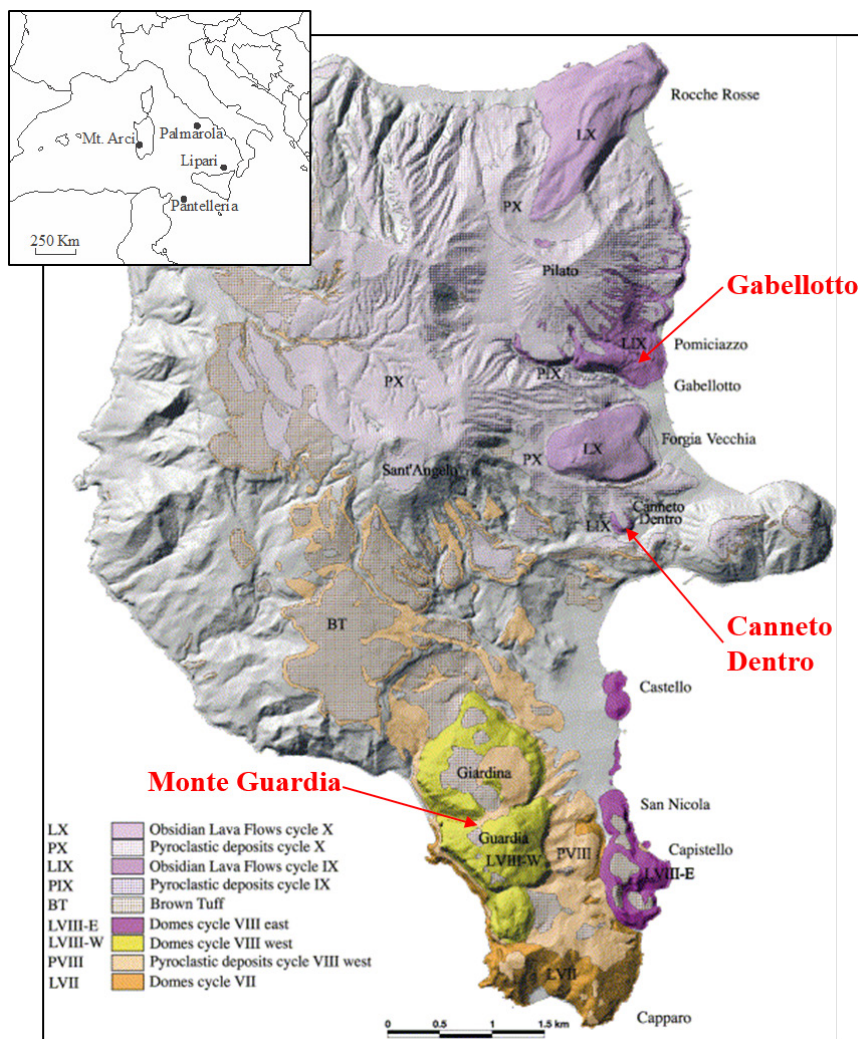

Figure 1. Geological map of Lipari draped on a DEM shaded relief image (modified after Pichler, 1980, Crisci et al., 1991, and Gioncada et al., 2003). The flows for Gabellotto Gorge and Canneto Dentro are dated to the LIX (obsidian lava flows cycle IX) volcanic event.

Radiocarbon dating has been used to date the Vallone del Gabellotto-Monte Pilato marker bed to 8.7–8.4 kya (Gioncada et al., 2003, p. 198; Forni et al., 2013, pp. 246–247), but this date is based on a single radiocarbon date of 7770 ± 70 obtained on foraminifera from an Adriatic Sea core with rhyolitic tephra named E-1 which is attributed to the Gabellotto eruption (Siani et al., 2004; Zanchetta et al., 2011). The 2-sigma calibrated range of 6780–6450 cal BC for this sample is just a few hundred years prior to the beginning of the Early Neolithic in southern Italy. The Vallone Canneto Dentro eruptive formation is stratigraphically beneath that of Gabellotto, but has not been directly dated. It is only exposed now in a small area to the southeast of Gabellotto.

Volcanic activity on Lipari was quiescent then until historic times when eruptions from the side of Mt. Pelato in the northeastern quarter of Lipari buried much of the prehistoric archaeological record with up to 300 meters of pumice and other volcanic debris, first at Forgia Vecchia about 776 AD, and then at Rocche Rosse-Lami about 1200 AD (Forni et al., 2013). The obsidian produced in these historical eruptions is of comparable high quality and size, making it easily confused visually with that of prehistoric age. Obsidian also formed on the island of Vulcano in the 1700s AD.

3 Archaeological Background

Lipari appears to have been first settled in the Early Neolithic, ca. 5500 BC, in parallel to the westward spread from the Eastern Mediterranean of domesticated plants and animals, and use of ceramics. The excavated Middle Neolithic (Stentinello culture) site of Castellaro Vecchio in Quattropani, and the Late Neolithic site (Diana culture) of Contrada Diana, have revealed extensive obsidian production at a scale far beyond the needs of the modest number of people living on Lipari (Bernabò Brea & Cavalier, 1957, 1960; Martinelli, 2016; Martinelli et al., 2019). Unfortunately, our knowledge of activity on Lipari itself will remain limited due to the destruction and/or coverage by pumice from the historic eruptions.

The earliest known evidence of the exploitation of Lipari obsidian comes from artifacts at sites in Sicily and mainland Italy dating to the beginning of the Early Neolithic, ca. 6000 BC. This is suggestive that the knowledge of the Gabellotto obsidian flow was acquired relatively quickly after the eruption of Mt. Pelato in the Late Mesolithic, with visits to Lipari part of the overall exploration and settlement by agriculturalists at the beginning of the Neolithic. This appears to coincide with the earliest use of obsidian from Palmarola, Pantelleria, and Sardinia as well. By slightly later phases of the Early Neolithic, Lipari obsidian was distributed to sites throughout the Italian peninsula, into southern France, and across the Adriatic to Croatia (Crisci et al., 1994; De Francesco et al., 2011; Tykot, 2017a).

Archaeologists and geologists have generally thought that the obsidian flow which was utilized during the Neolithic period is today primarily exposed only in the Gabellotto Gorge area along the southern edge of Mt. Pelato.

4 Field Survey

Starting in 2000, a field survey on Lipari was initiated with permission from the Soprintendenza della Provincia di Messina, and funding from the National Science Foundation (BCS-0075535) as part of a larger study that also included the obsidian sources and subsources on the islands of Palmarola and Pantelleria. The members of the team collected obsidian geological materials during field visits to Lipari in 2000, 2001, 2002, and 2005. The team surveyed and collected more than 1300 geological specimens of obsidian from both previously identified well-known locations as well as new find spots (Figure 2). The waypoints of more than 40 findspots were recording using GPS, including Canneto Dentro, Forgia Vecchia, Gabellotto, Pomiciazzo, Monte Guardia, Rocche Rosse, and others along the northern and eastern coast and inland areas of Lipari (Figures 3–7).
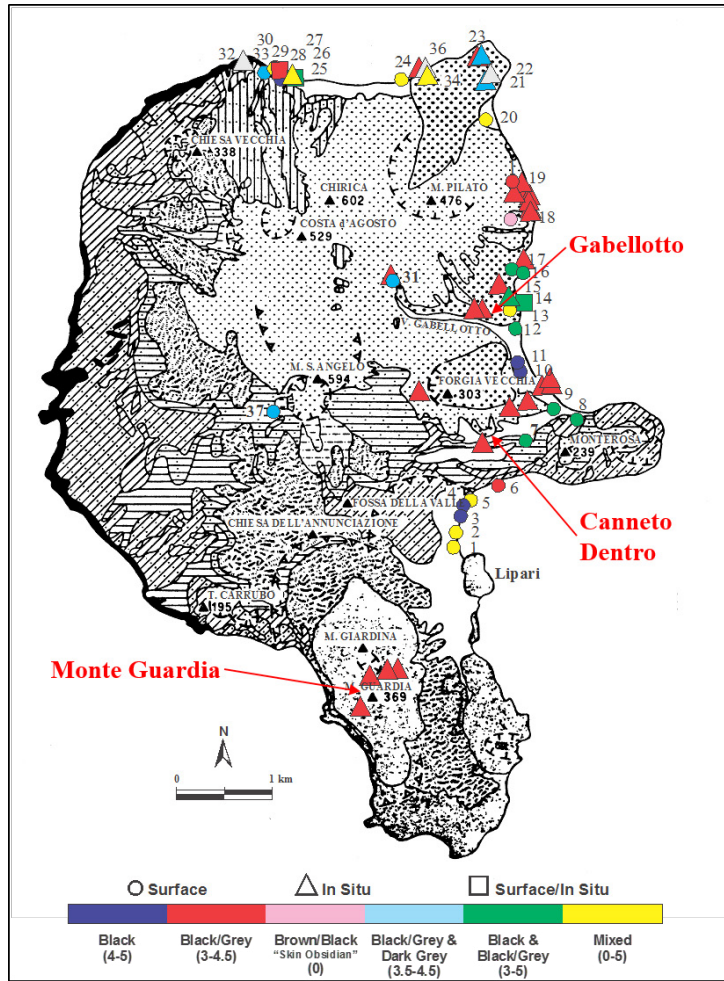
Figure 2. Lipari localities of geological samples collected.

Figure 3. Picture of Gabellotto Gorge from the northwest. Monte Rosa in the background.

Figure 4. Picture of Gabellotto Gorge outcrop.

Figure 5. Lipari coast with obsidian. Picture from north with Monte Rosa in the background.

Figure 6. Obsidian deposits exposed by modern construction activities.

Figure 7. Obsidian block near Roche Rosse.

A detailed photographic record was taken along with field logs recording each locality, the quality, quantity, and size of the obsidian nodules collected as well as its geological depositional context, i.e., whether it was in an in situ or secondary deposit. Subsequently in the laboratory, the specimens were weighed and photographed digitally, and small sections of 1 gram each were removed with a diamond saw, ultrasonically cleaned, and later oven-dried in preparation for density measurements to be taken. The density was obtained by measuring the dry mass and the suspended wet weight in a water/PV wetting solution. When the density values are compared with those for the other central Mediterranean island sources, Lipari obsidian has the lowest and mostly can be differentiated from Palmarola and Sardinia (Figure 8). Lipari obsidian is often very glassy, while Pantelleria obsidian is much denser, and the least brittle.

Visual descriptions were made for obsidian, specifically transparency, luster, color, type and color of any inclusions or patterning, e.g., banding, mottling, or streaking that may have been present. Lipari obsidian has a wide range of transparency, from opaque to highly transparent, with those in the opaque

category often having extensive phenocrysts. The luster is typically high, while all are in the dark gray-to-black range of color; there is significant variation in the color patterns, including uniform, banded, streaked, and mottled, but nearly all with a smooth texture. These varieties were used for producing obsidian cores and stone tools (Figures 9–10).
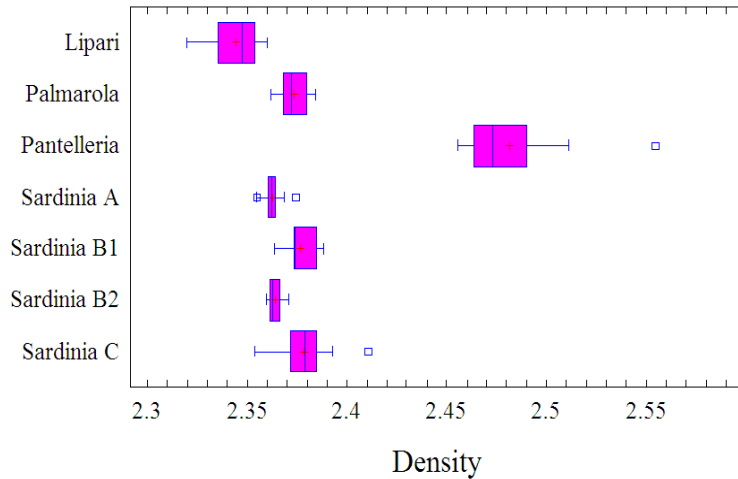

Figure 8. Box plot of density for central Mediterranean obsidian geological samples.

Figure 9. Selection of obsidian cores found on Lipari.

Figure 10. An obsidian assemblage from Lipari.

5 Obsidian Source Characterization

Cann & Renfrew (1964) first demonstrated that many of the European/Near Eastern obsidian sources could be differentiated based on their trace element composition (especially barium, zirconium, niobium and yttrium) as determined by optical emission spectroscopy, while earlier studies by Cornaggia Castiglioni et al. (1962, 1963) which used manganese and other major elements were promising in the Mediterranean but had some erroneous attributions. By the mid-1970s, the use of X-ray fluorescence spectrometry and instrumental neutron activation analysis were each shown to be quite successful in attributing artifacts to specific Mediterranean islands, and illustrating the long-distance distribution of artifacts from these sources in the neolithic (Hallam et al., 1976; Francaviglia, 1984). Since then, additional analytical methods have been successfully used, including major/minor element analyses using scanning electron microscopes (SEM) with energy-dispersive (ED) or wavelength dispersive (WD) spectrometers (Le Bourdonnec et al., 2006; Tykot, 1997), and trace element analyses using atomic absorption spectroscopy (AAS), inductively coupled plasma emission spectrometry (ICP-OES, ICP-AES) and mass spectrometry (ICP-MS), often with a laser (Barca et al., 2007; Tykot, 2002, 2004). While all of these methods have been used successfully, the size of archaeological research projects had been limited due to the accessibility, cost and destructive nature of most analytical methods. The 21st century development of non-destructive XRF instruments, especially portable types, has changed that entirely with many thousands of artifacts from the central Mediterranean now tested (De Francesco et al., 2011; Le Bourdonnec, 2007; Pappalardo et al., 2013; Poupeau et al., 2009; Tykot 2017a, b).

It is important from an archaeological perspective to have detailed information on the actual location(s) where obsidian was obtained, and not just attribute artifacts to a general geological region or island. Elsewhere in the Mediterranean, attributing archaeological samples to specific island subsources already has been shown to be extremely important for understanding the actual acquisition of the raw materials, including the physical travel and transport involved; differences in the quantity, quality, and visual characteristics between different outcrops or subsources; and whether acquisition was done by local residents, perhaps with territorial control of access, or by visitors whether local or from elsewhere. For Monte Arci on Sardinia, it has been shown that the usage of obsidian from three subsources (SA, SB2, SC) changed over the course of the Neolithic (Tykot, 1997), while for Melos in the Aegean the subsources of Sta Nychia and Dhemenegaki were also used in different proportions with changes over time (Carter & Kilikoglou, 2007).

The transport and distribution of obsidian found at mainland sites was complex, and involved at least three separate steps of travel: from island source locale over land to the coast, carried by people and possibly oxen; over water, in some kind of raft or vessel; and back on land from coast to archaeological site, perhaps with different people and/or oxen, especially if over lengthy distances.

6 Lipari Obsidian Analysis

A statistically significant selection of the approximately 1300 geological samples collected during the Lipari survey were initially analyzed by INAA, LA-ICP-MS, and ED-XRF at the Missouri University Research Reactor (Speakman et al., 2007). Many of the same samples were analyzed by the different methods. Details on the sample preparation and analysis by these instruments are provided in Appendix. Each of these analytical methods revealed elemental differences between Gabellotto Gorge and Canneto Dentro, as well as with the earlier Monte Guardia and later Forgia Vecchia and Rocche Rosse deposits (Tykot et al., 2006). There are also two chemical groups for Gabellotto Gorge, one for the north area and one in the base of the gorge.

Neutron activation analysis was conducted on 159 geological samples, including 39 of prehistoric age. The prehistoric Lipari obsidian subgroups of Monte Guardia, Gabellotto (base and north), and Canneto Dentro are distinguishable using several different trace elements, with clear differences for La, Ce, and Co (Figure 11).
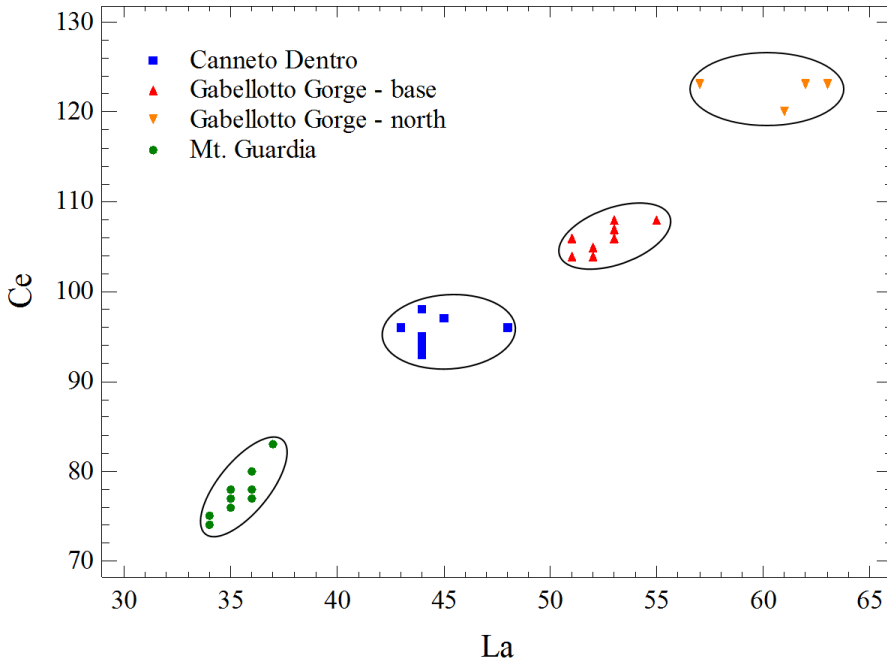
Figure 11. X-Y graph of Lipari subsources using INAA on trace elements lanthanum and cerium.

Laser ablation ICP mass spectrometry was performed on 213 geological samples, including 49 of prehistoric age. Multi-variate discriminant function statistical analysis clearly distinguishes not only the prehistoric subgroups of Monte Guardia, Gabellotto (base and north), and Canneto Dentro, but also the historic Forgia Vecchia and Rocche Rosse subsources (Figures 12–13).

Energy-dispersive X-ray fluorescence analysis was performed on 110 geological samples, with 20 of prehistoric age. While the ED-XRF is as successful as INAA and LA-ICP-MS in discriminating the Lipari subsources, subsequent non-destructive XRF analyses have been conducted with a portable model.
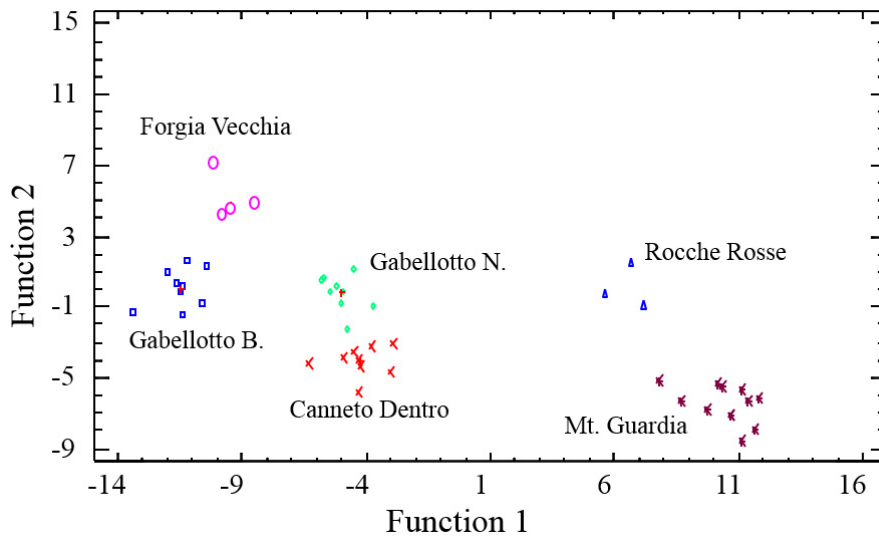
Figure 12. Discriminant function graph of prehistoric and historic Lipari subsources by LA-ICP-MS.
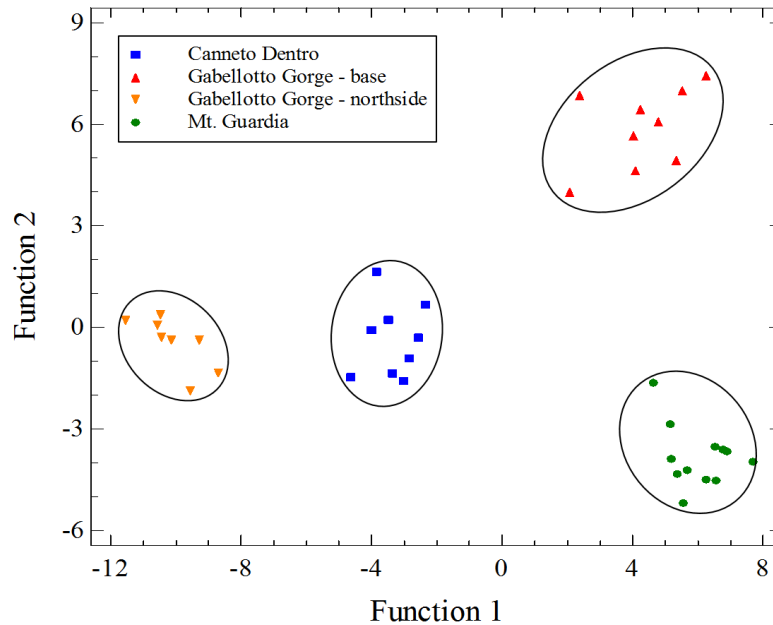
Figure 13. Discriminant function graph of prehistoric Lipari subsources by LA-ICP-MS.

Over the past ten years, the pXRF analyses were conducted using different models of the Bruker Tracer, including the III-V+, III-SD, and V*i*. The settings have remained fairly similar, using a Cu-Ti-Al filter to reduce the background and increase the precision of the K-alpha peaks for Fe through Rb, while running at 40–50 kV and 10–35 μA for 180 to 30 seconds. In each case, the results are calibrated using a large number of obsidian standards provided by MURR (Missouri University Research Reactor) and run directly on each instrument (Tykot, 2017b). When using the pXRF, which produces quantitative data on fewer trace elements than the other methods, assignment of an artifact to a specific Lipari subsource is dependent mainly on the concentration of strontium, with the base of Gabellotto ~20 ppm, the northern area of Gabelloto ~30–35 ppm, and at Canneto Dentro ~40–70 ppm. More than 60 prehistoric geological subsource samples have been tested by pXRF (Figure 14).
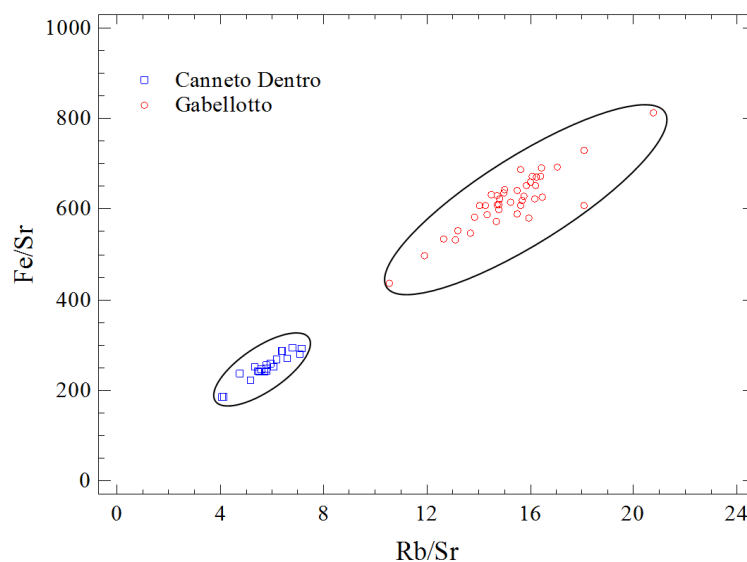
Figure 14. Element ratios for Canneto Dentro and Gabellotto Gorge by pXRF.

7 Discussion

Many thousands of prehistoric obsidian artifacts from central Mediterranean sites in Sicily, Malta, Ustica, Croatia, and throughout peninsular Italy, as well as at some sites in Corsica and southern France, have been analyzed and assigned to Lipari (Tykot, 2017a; Freund, 2018) (Figure 15). The predominance of Lipari obsidian in lithic assemblages in Sicily and Calabria is of no surprise given their modest distances from this Aeolian island and the apparent regularity of sea travel and mobility during the Neolithic in this region (see also Ammerman, 1985; Robb & Farr, 2005). It is only about 20 km open water from Lipari to the tip of Milazzo in northern Sicily, while it appears that regular sea travel over much greater distances occurred regularly by the beginning of the neolithic, with settlements and domestic animals on Malta (80 km), Ustica (52 km), and many other islands in the Mediterranean. In general, it appears that obsidian cores were produced on Lipari and regularly brought to Sicily and Calabria where they were used to produce blades.

Figure 15. Sites with Lipari obsidian and ≥10 artifacts analysed.

The distribution during the Neolithic of Lipari obsidian in small quantities as far as southern France has also been known for some time, and this may be thought to have been exotic items that made their way to the fringes of obsidian distribution (Tykot, 2011). Significant quantities of Lipari obsidian, however, have been found on the Croatian side of the Adriatic Sea (Tykot, 2014), and at several sites in central and northern Italy, including Poggio Olivastro, Pescale, and four near Parma (Tykot et al., 2018), expanding considerably the geographic area in which obsidian regularly was distributed during the Neolithic, perhaps to some inland sites which served as centers for redistribution.

Important to note is that it appears from these thousands of analyses of obsidian artifacts that came from Lipari that the major source locality was the base of Gabellotto Gorge. Only very small percentages from the north area of Gabellotto, and from Canneto Dentro, were utilized in the past. Low percentages of Canneto Dentro obsidian artifacts have been identified at many sites in Sicily, but none at all identified in Malta, or on Ustica. For peninsular Italy, Canneto Dentro obsidian has been identified at 6 different sites in Calabria and Campania, but only 8 artifacts in total and 0.3% of the total number of the obsidian artifacts from these regions assigned to Lipari. Further interpretation of these data, with comparisons between different chronological phases of the Neolithic, may suggest that this is related to the development of territorial control and organized production within Lipari.

8 Conclusions

While our recognition of the long-distance distribution of obsidian from Lipari has become quite well-established, there had been several other important questions that needed to be addressed, including how and where the obsidian was actually obtained on Lipari, and whether that may have changed over time as has been shown for the Monte Arci subsources on Sardinia (Tykot, 1996). In this study, the results of the detailed collection and elemental analysis of geological obsidian samples throughout the island of Lipari demonstrated that specific outcrop areas of obsidian available in prehistoric times could be distinguished from each other, as well as from the historic eruptions, using rapid non-destructive analyses with a portable XRF, as well as by INAA and LA-ICP-MS.

The analyses of many thousands of artifacts from sites throughout Italy and neighboring countries has revealed none attributed to Monte Guardia, apparently due to the only small-size geological pieces found there, while the low percentage of artifacts attributed to Canneto Dentro was expected given its quite modest exposed geographic area relative to the large Gabellotto Gorge area still accessible today. Nevertheless, the infrequent apparent use of Canneto Dentro obsidian on and off Lipari may enlighten our understanding of the *chaîne opératoire* of selection, production, and distribution established in the Early Neolithic and how that may have changed over the following several thousand years in the central Mediterranean. The assessment of whether pre-formed cores were only produced on Lipari, or natural blocks were transported to Sicily or mainland Italy, may be related to who was involved in the initial acquisition, i.e. island residents or irregular visitors, and the overall purpose and frequency of their maritime travels. There is no question that the quantity of obsidian working evident by the Middle Neolithic at Castellaro Vecchio indicates major production on Lipari for export.

Understanding the role of obsidian in the development of cultural and economic complexity on the island of Lipari is central to our reconstruction of the social dynamics of a broader regional exchange network in the central Mediterranean, especially that in Sicily, nearby islands, and southern peninsular Italy during the Neolithic. The identification of Lipari obsidian artifacts at more than 200 archaeological sites in the central Mediterranean is important for understanding patterns of culture contact, maritime capabilities and levels of socio-economic organization as they may have changed over the course of the Neolithic period. Obsidian also acts as a proxy for materials less visible in the archaeological record when reconstructing contact networks. Being able to distinguish between obsidian subsources, and whether certain patterns were characteristic of specific time periods, provides some insight into the cultural, economic, and political complexity of prehistoric Lipari.

Note: A complete database of the geological samples, representing both prehistoric and historic time periods, and including GPS location, size and weight measurements, detailed visual description, and analytical data is available upon request.

References

Ammerman, A.J. (1985). The Acconia Survey: Neolithic Settlement and the Obsidian Trade. Lonon: Institute of Archaeology, University of London.

Arias-Radi, G., Bigazzi, G., & Bonadonna, F. (1972). Le tracce di fissione: Un metodo per lo studio delle vie di commercio dell'ossidiana. Origini: Preistoria e Protostoria delle civiltà antiche, 6, 155–169.

Arias, C., Bigazzi, G., Bonadonna, F. P., Cipolloni, M., Hadler, J. C., Lattes, C. M. G., & Radi, G. (1984). Fission track dating in archaeology, a useful application. In P. L. Parrini (Ed.), Scientific methodologies applied to works of art (pp. 151–159).

Barca, B., De Francesco, A.M., & Crisci, G.M. (2007). Application of Laser Ablation ICP-MS for characterization of obsidian fragments from peri-Tyrrhenian area. Journal of Cultural Heritage, 8(2), 141–150.

Bernabò Brea, L., & Cavalier, M. (1957). La stazione stentinelliana del Castellaro Vecchio presso Quattropani (Lipari). Bullettino di Paletnologia Italiana, 66, 97–151.

Bernabò Brea, L., & Cavalier, M. (1960). La stazione preistorica della Contrada Diana e la necropoli protostorica di Lipari. Meligunis Lipara I. Flaccovio, Palermo.

Bigazzi, G., & Bonadonna, F. (1973). Fission Tracking Dating of the Obsidian of Lipari Island (Italy). Nature, 242, 322–323.

Cann, J.R., & C. Renfrew. (1964). The characterization of obsidian and its application to the Mediterranean region. Proceedings of the Prehistoric Society, 30, 111–33.

Carter, T., & Kilikoglou, V. (2007). From Reactor to Royalty? Aegean and Anatolian Obsidians from Quartier Mu, Malia (Crete). Journal of Mediterranean Archaeology, 20.1, 115–143.

Cornaggia Castiglioni, O., Fussi, F., & D'Agnolo, M. (1962). Indagini sulla provenienza dell'ossidiana in uso nelle industrie preistoriche italiane. Atti della Società Italiana di Scienze Naturali e del Museo Civico di Storia Naturale in Milano, 101, 12–19.

Cornaggia Castiglioni, O., Fussi, F., & D'Agnolo, M. (1963). Indagini sulla provenienza dell'ossidiana utilizzata nelle industrie preistoriche del Mediterraneo occidentale. Atti della Società Italiana di Scienze Naturali e del Museo Civico di Storia Naturale in Milano, 102, 310–22.

Crisci, G.M., De Rosa, R., Esperanca, S., Mazzuoli, R., & Sonnino, M. (1991). Temporal evolution of a three component system: the island of Lipari (Aeolian Arc, southern Italy). Bulletin of Volcanology, 53, 207–221.

Crisci, G.M., Ricq-de Bouard, M., Lanzaframe, U., & De Francesco, A.M. (1994). Les obsidiennes du midi de la France. Gallia Preistoire, 36, 299–327.

De Francesco, A.M., Bocci, & G. M. Crisci. (2011). Non-destructive applications of wavelength XRF in obsidian studies in X-ray fluorescence spectrometry (XRF) in geoarchaeology. In M. S. Shackley (Ed.), X-Ray Fluorescence Spectrometry (XRF) in Geoarchaeology. (pp. 81–107). New York: Springer.

Forni, F., Lucchi, F., Peccerillo, A., Tranne, C.A., Rossi, P.L., & Frezzotti, M.L. (2013). Stratigraphy and geological evolution of the Lipari volcanic complex (cental Aeolian archipelago). In F. Lucchi, A. Peccerillo, J. Keller, CA. Tranne, P.L. Rossi (Eds.), The Aeolian Islands Volcanoes. (pp. 213–279). London: Geological Society.

Francaviglia, V.M. (1984). Characterization of Mediterranean obsidian sources by classical petrochemical methods. Preistoria Alpina, 20, 311–332.

Freund, K.P. (2018). A long-term perspective on the exploitation of Lipari obsidian in central Mediterranean prehistory. Quaternary International, 468, 109–120.

Gioncada, A., Mazzuoli, R., Bisson, M., & Pareschi, M.T. (2003). Petrology of volcanic products younger than 42 ka on the Lipari-Vulcano complex (Aeolian Islands, Italy): an example of volcanism controlled by tectonics. Journal of Volcanology and Geothermal Research, 122, 191–220.

Gratuze, B., Blet-Lemarquand, M., & Barrandon, J.N. (2001). Mass spectrometry with laser sampling: A new tool to characterize archaeological materials. Journal of Radioanalytical and Nuclear Chemistry, 247 (3), 645–656.

Hallam, B.R., Warren, S.E., & Renfrew, C. (1976). Obsidian in the western Mediterranean: chacterisation by neutron activation analysis and optical emission spectroscopy. Proceedings of the Prehistoric Society, 42, 85–110.

Keller, J. (1970). Datierung der Obsidiane und Bimstuffe von Lipari. Neues Jahrbuch fur Geologie und Palaontologie, Monatshefte, 1, 90–101.

Le Bourdonnec, F.-X. (2007). Aspects archéométriques de la circulation de l'obsidienne préhistorique: Développements analytiques et applications en Corse, Sardaigne et Éthiopie. PhD dissertation, Université Michel de Montaigne Bordeaux 3, France.

Le Bourdonnec, F.-X., Poupeau, G., & Luglie, C. (2006). SEM-EDS analysis of western Mediterranean obsidians: a new tool for Neolithic provenance studies. C. R. Geoscience, 338, 1150–1157.

Martinelli, M.C. (2016). Updates on the cultural and chronological framework of the prehistory and protohistory of the Aeolian Islands: from the first settlement to the end of the villages. In Cazzella, A., Guidi, A., Nomi, F. (eds.) Convegno di studi in memoria di Giorgio Buchner "Ubi minor.. le isole minori del Mediterraneo centrale dal Neolitico ai primi contatti coloniali", Capri - Anacapri - Ischia 27-29 ottobre 2013, Scienze dell'Antichità, Roma, 263–279.

Martinelli, M.C., Tykot, R.H., Vianello, A. (2019). Lipari (Aeolian Islands) Obsidian in the Late Neolithic. Artifacts, Supply and Function. Open Archaeology, 5, 46–64.

Pappalardo, L., Romano, F. P., Bracchitta, D., Massimino, A., Palio, O., & Rizzo, F. (2013). Obsidian provenance determination using the beam stability controlled BSC-XRF and the PIXE-alpha portable spectrometers of the LANDIS laboratory: the case of Via Capuana settlement in Licodia Eubea (Sicily). Journal of Geophysics and Engineering, 10, 1–12.

Pichler, H. (1980). The Island of Lipari. Rendiconti Societa Italiana di Mineralogia e Petrologia, 36, 415–440.

Poupeau, G., Le Bourdonnec, F.-X., Dubernet, S., & Delerue, S. (2009). Instrumental methods of obsidian characterization and prehistoric obsidian provenance studies: The current status. In S. Farina, L. Eigeland, L.-J. Costa (Eds.), Non-Flint Raw Material Use in Prehistory: Old prejudices and new directions. Proceedings of the XV World Congress (Lisbon, 4-9 September 2006). (pp. 35–42). Oxford: Archaeopress.

Robb, J.E., & Farr, R.H. (2005). Substances in motion: neolithic Mediterranean "Trade". In E. Blake, & A. B. Knapp (Eds.), The Archaeology of Mediterranean Prehistory. (pp. 24–46). Chichester, GB: Blackwell Publishing Ltd.

Siani, G., Sulpizio, R., Paterne, M., & Sbrana, A. (2004) Tephrostratigraphy study for the last 18,000 14C years in a deep-sea sediment sequence for the South Adriatic. Quaternary Science Reviews, 23, 2485–2500.

Speakman, R.J., Glascock, M.D., Tykot, R.H, Descantes, C., Thatcher, J.J., Skinner, C.E., & Lienhop, K.M. (2007). Selected Applications of Laser Ablation Inductively Coupled Plasma-Mass Spectrometry Archaeological Research. In M.D. Glascock, R.J. Speakman & R.S. Popelka-Filcoff (eds.), Archaeological Chemistry: Analytical Techniques and Archaeological Interpretation. ACS Symposium Series, 968, 275–296. Washington, DC: American Chemical Society.

Tykot, R.H. (1996). Obsidian Procurement and Distribution in the Central and Western Mediterranean. Journal of Mediterranean Archaeology, 9(1), 39–82.

Tykot, R.H. (1997). Characterization of the Monte Arci (Sardinia) obsidian sources. Journal of Archaeological Science, 24, 467–479.

Tykot, R.H. (2002). Chemical fingerprinting and source-tracing of obsidian: The central Mediterranean trade in black gold. Accounts of Chemical Research, 35, 618–627.

Tykot, R.H. (2004). Scientific methods and applications to archaeological provenance studies. In M. Martini, M. Milazzo, M. Piacentini (Eds.), Physics Methods in Archaeometry. Proceedings of the International School of Physics "Enrico Fermi" Course CLIV. (pp. 407–432). Bologna, Italy: Società Italiana di Fisica.

Tykot, R.H. (2011). Obsidian finds on the fringes of the central Mediterranean: Exotic or eccentric exchange? In A. Vianello (Ed.), Exotica in the Prehistoric Mediterranean. (pp. 33–44). Oxbow Books.

Tykot, R.H. (2014). Obsidian use and trade in the Adriatic. In P. Visentini and E. Podrug (Eds.), The Adriatic, a sea without borders: communication routes of populations in 6000 BC. (pp. 171–181, 224-225). Civici Musei di Udine, Museo Friulano di Storia Naturale.

Tykot, R.H. (2017a). Obsidian Studies in the Prehistoric Central Mediterranean: After 50 Years, What Have We Learned and What Still Needs to Be Done? Open Archaeology, 3, 264–278.

Tykot, R.H. (2017b). A Decade of Portable (Hand-Held) X-Ray Fluorescence Spectrometer Analysis of Obsidian in the Mediterranean: Many Advantages and Few Limitations. MRS Advances, 2(33-34), 1769–1784.

Tykot, R.H., Freund, K.P., & Vianello, A. (2013). Source analysis of prehistoric obsidian artifacts in Sicily (Italy) using pXRF. In R.A. Armitage, J.H. Burton (Eds.), Archaeological Chemistry VIII. ACS Symposium Series, 1147, 195–210.

Tykot, R.H., Freund, K.P., & Vianello, A. (2018). Obsidian Distribution in the Western Mediterranean and the Spread of the Neolithic Package: A Chronological and Geographical Comparison. 24th EAA Annual Meeting: Reflecting Futures (Barcelona, 2018) - Abstract Book, 2, 1116.

Tykot, R.H., Iovino, M.R., Martinelli, M.C., & Beyer, L. (2006). Ossidiana da Lipari: le fonti, la distribuzione, la tipologia e le tracce d'usura. Atti del XXXIX Riunione Scientifica dell'Istituto Italiano di Preistoria e Protostoria: Materie prime e scambi nella preistoria italiana, Firenze, 25-27 November 2004. (pp. 592–597). Firenze.

Wagner, G.A., Storzer, D., & Keller, J. (1976). Spaltspurendatierung Quartarer Gesteinsglaser aus dem Mittelmeerraum. Neues Jahsbuch for Mineralogie Monatslefle, 1976(2), 84–94.

Zanchetta, G., Sulpizio, R., Roberts, N., Cioni, R., Eastwood, W.J., Siani, G., Caron, B., Paterne, M., & Santacroce, R. (2011). Tephrostratigraphy, chronology and climatic events of the Mediterranean basin during the Holocene: An overview. The Holocene, 21(1), 33–52.

Appendix. Instrumental Analyses

Analysis by INAA at MURR

The obsidian samples were crushed to create a number of interior fragments (approx. 25–50 mg in size). The fragments were inspected under a magnifier to eliminate those with crush fractures, metallic streaks, etc. Two subsamples were prepared for INAA short and long irradiations. The first sample (~100 mg) was placed into a clean polyethylene vial, while the second sample (250–300 mg) was placed into a high-purity quartz vial. The short irradiation samples were sequentially irradiated for five seconds each in a neutron flux of 8 x 1013 neutrons cm-2 s-1 and then decayed for 25 minutes before being counted for 12 minutes with a high-purity germanium (HPGe) detector. The short-lived elements Ba, Cl, Dy, K, Mn and Na were measured in most samples. The long irradiation samples were irradiated in bundles of 30–35 samples each for 70 hours in a neutron flux of 5 x 1013 neutrons cm-2 s-1. After decaying for about eight days, the long irradiation samples were loaded on a sample changer where they were counted for 2,000 seconds each to measure the medium-lived elements Ba, La, Lu, Nd, Sm, U, and Yb. In most cases, the value for Ba determined from long irradiation was superior to that measured by short irradiation. Three weeks afterwards the long irradiation samples were counted again for 10,000 seconds to measure the long-lived elements Ce, Co, Cs, Eu, Fe, Hf, Rb, Sb, Sc, Sr, Ta, Tb, Th, Zn and Zr. Standards made from SRM-278 Obsidian Rock and SRM-1633a were similarly prepared and irradiated for calibration and quality control of the analytical data.

Table 1. INAA analyses of Lipari subsources.

USF #	Area	Sc	Fe	Co	Zn	Rb	Sr	Zr	Sb	Cs	Ba	La	Ce	Nd	Sm	Eu	Tb	Yb	Lu	Hf	Ta	Th	U
4560	Mt. Guardia	0,93	9939	0,19	49	280	0	217	0,93	15,0	54	35	77	29	7,5	0,11	1,05	4,0	0,78	5,5	2,20	39	12,0
4565	Mt. Guardia	0,93	9986	0,20	49	286	0	218	0,91	15,1	42	35	76	31	7,6	0,11	1,05	4,0	0,76	5,5	2,24	39	11,9
4574	Mt. Guardia	1,06	10301	0,22	52	285	0	217	0,91	15,3	75	35	78	27	7,6	0,11	1,08	4,1	0,73	5,6	2,28	39	11,8
4590	Mt. Guardia	1,08	10355	0,21	52	288	0	213	0,91	15,1	62	35	78	30	7,7	0,11	1,06	3,9	0,78	5,8	2,23	39	11,9
4594	Mt. Guardia	1,20	10113	0,21	51	278	0	217	0,97	14,7	66	34	75	28	7,4	0,12	1,06	4,0	0,76	5,9	2,23	38	11,7
4597	Mt. Guardia	1,01	10091	0,21	49	283	0	212	0,90	15,0	69	35	76	30	7,7	0,11	1,06	4,1	0,77	5,5	2,23	39	11,7
4600	Mt. Guardia	0,93	10131	0,20	49	286	0	212	0,94	15,2	51	35	78	28	7,6	0,11	1,04	4,1	0,76	5,6	2,25	39	12,4
4615	Mt. Guardia	0,97	10309	0,20	51	289	0	216	0,95	15,5	57	36	80	30	7,6	0,11	1,06	4,2	0,77	5,7	2,25	40	12,3
4620	Mt. Guardia	0,93	10164	0,21	50	289	0	237	0,91	15,2	48	36	78	31	7,7	0,11	1,07	4,1	0,76	5,5	2,24	39	12,3
4638	Mt. Guardia	0,99	10225	0,21	49	290	0	225	0,94	15,0	45	34	74	29	7,2	0,11	1,01	3,9	0,72	5,6	2,27	39	12,5
4639	Mt. Guardia	0,90	9876	0,19	51	282	0	218	0,92	14,9	55	36	77	31	7,5	0,12	1,04	3,9	0,73	5,7	2,21	39	12,4
4658	Mt. Guardia	0,95	10282	0,22	52	289	0	210	0,87	15,4	0	37	83	33	8,2	0,12	1,09	4,2	0,83	5,6	2,24	40	12,7
4688	Canneto Dentro	1,70	12183	1,12	54	289	21	266	0,97	15,4	84	48	96	37	8,0	0,16	1,05	4,1	0,77	6,5	2,30	45	13,5
4689	Canneto Dentro	2,42	13662	1,78	56	282	91	296	1,00	15,2	90	44	93	30	8,2	0,20	1,06	4,6	0,77	6,6	2,20	45	12,9
4694	Canneto Dentro	1,35	12255	0,85	58	297	88	266	1,04	16,1	105	44	98	34	8,4	0,16	1,13	4,8	0,78	6,4	2,33	47	13,8
4696	Canneto Dentro	1,56	11774	0,91	52	289	-	263	1,00	15,7	62	44	95	32	8,3	0,16	1,07	4,8	0,82	6,3	2,24	47	13,5
4699	Canneto Dentro	1,66	12187	1,34	51	280	18	243	0,97	15,2	60	44	94	31	8,2	0,16	1,06	4,4	0,80	6,1	2,19	45	14,1
4702	Canneto Dentro	1,76	12505	1,25	57	284	33	262	0,97	15,4	54	43	96	31	8,3	0,17	1,04	4,8	0,79	6,2	2,20	46	13,2
4705	Canneto Dentro	1,51	12144	1,06	55	285	31	250	1,00	15,5	94	44	94	31	8,2	0,16	1,08	5,5	0,78	6,1	2,23	46	13,1
4706	Canneto Dentro	1,74	12577	1,16	56	290	82	298	1,00	15,7	68	45	97	36	8,3	0,18	1,10	4,6	0,81	6,6	2,29	47	13,8
4710	Canneto Dentro	2,17	12791	1,43	58	290	91	258	0,98	15,8	66	44	95	34	8,3	0,18	1,07	5,3	0,81	6,3	2,25	47	13,9
4817	Gabellotto Gorge - north	1,13	12078	0,39	61	301	0	302	1,08	16,9	107	57	123	42	9,3	0,15	1,12	5,0	0,83	7,0	2,42	54	15,0

continued**Table 1.** INAA analyses of Lipari subsources.

USF #	Area	Sc	Fe	Co	Zn	Rb	Sr	Zr	Sb	Cs	Ba	La	Ce	Nd	Sm	Eu	Tb	Yb	Lu	Hf	Ta	Th	U
4818	Gabellotto Gorge - north	1,09	11539	0,38	61	292	0	288	1,06	16,2	92	61	120	41	8,6	0,15	1,06	4,1	0,80	6,7	2,39	50	14,8
4819	Gabellotto Gorge - north	1,11	11801	0,37	61	296	0	309	1,07	16,4	84	63	123	45	8,8	0,14	1,11	4,1	0,81	6,9	2,40	51	14,9
4820	Gabellotto Gorge - north	1,11	11805	0,37	61	299	0	295	1,09	16,5	64	62	123	38	8,7	0,15	1,09	4,2	0,80	6,9	2,43	50	14,8
4821	Gabellotto Gorge - north	1,12	11983	0,37	61	300	0	283	1,14	16,7	55	63	123	40	8,8	0,14	1,09	4,1	0,79	6,9	2,47	51	14,7
4825	Gabellotto Gorge - base	0,95	11303	0,32	57	295	0	275	1,06	15,9	78	53	106	39	8,5	0,14	1,09	4,0	0,79	6,6	2,36	47	14,0
4826	Gabellotto Gorge - base	0,98	11556	0,35	58	296	0	281	1,07	16,1	82	55	108	37	8,6	0,13	1,12	4,2	0,81	6,7	2,43	48	15,2
4827	Gabellotto Gorge - base	0,95	11321	0,36	54	299	0	298	0,96	16,1	82	53	107	40	8,5	0,13	1,10	4,3	0,88	6,6	2,40	48	14,2
4828	Gabellotto Gorge - base	0,96	11191	0,33	58	293	0	289	1,12	15,8	82	53	106	32	8,3	0,14	1,07	4,0	0,78	6,5	2,34	47	14,6
5841	Gabellotto Gorge - base	0,94	11151	0,34	56	290	0	279	0,96	15,8	66	51	104	33	8,0	0,13	1,07	4,1	0,78	6,5	2,36	47	13,6
5842	Gabellotto Gorge - base	0,94	11213	0,34	53	287	0	259	0,93	15,7	74	52	104	36	7,9	0,13	1,08	3,9	0,81	6,5	2,29	47	14,0
5843	Gabellotto Gorge - base	0,93	11091	0,34	53	288	0	256	0,95	15,7	0	51	104	34	7,9	0,13	1,05	4,0	0,80	6,5	2,32	46	13,4
5844	Gabellotto Gorge - base	0,94	11113	0,33	53	289	0	279	0,98	15,7	62	51	104	38	8,0	0,13	1,09	4,0	0,81	6,5	2,33	47	13,1
5845	Gabellotto Gorge - base	0,96	11417	0,35	45	267	0	268	1,02	14,3	54	53	108	38	8,1	0,13	1,06	4,0	0,79	6,6	2,40	47	13,0
5846	Gabellotto Gorge - base	0,94	11166	0,33	54	289	0	262	0,92	15,8	76	52	104	40	7,9	0,13	1,04	4,1	0,79	6,5	2,34	47	13,4
5848	Gabellotto Gorge - base	0,94	11176	0,31	53	288	0	275	0,95	15,9	54	52	105	33	8,1	0,13	1,08	4,2	0,82	6,5	2,36	47	14,1
5849	Gabellotto Gorge - base	0,94	11235	0,33	53	290	0	275	0,96	15,8	53	51	106	38	8,1	0,13	1,08	4,2	0,80	6,7	2,36	47	14,1
5850	Gabellotto Gorge - base	0,94	11196	0,34	52	293	0	275	0,95	15,6	74	52	104	35	8,0	0,13	1,05	4,3	0,81	6,5	2,33	47	13,9

Analysis by LA-ICP-MS at MURR

The obsidian samples were analyzed by LA-ICP-MS using a Thermo Elemental Axiom high resolution magnetic sector ICP capable of resolving masses as close as 0.001 atomic mass units apart. The ICP-MS was coupled to a Merchantek Nd-YAG 213-nanometer laser ablation unit in which ~10 samples were mounted at any one time. The laser was operated at 80% power (~1.5 mJ) using a 200 Fm diameter beam, firing at 20 times per second. A rectangular raster pattern of approximately 4 mm^2 was drawn over a relatively flat spot on each sample. The laser scanned across the raster area at 70 Fm per second. The laser beam was allowed to pass over the ablation area one time prior to data acquisition in order to remove possible contaminants from the surface of the sample, to permit time for sample uptake, and for the argon plasma to stabilize after the introduction of fresh material. Analytes of interest were scanned three times and averaged. In most cases, the %RSD was 5–10%.

Standardization was accomplished by calibrating the instrument using NIST SRM-610 and SRM-612 glass wafers doped with 61 elements. Two obsidian glasses (from Glass Buttes, Oregon and Pachuca, Hidalgo, Mexico) calibrated in a round-robin exercise by the International Association of Obsidian Studies were also used. Monitoring the amount of material removed by the laser and transported to the ICP is complicated by several factors making normalization difficult. Conditions such as the texture of the sample, hardness of the sample, location of the sample in the laser chamber, laser energy, and other factors affect the amount of material

Table 2. LA-ICP-MS analyses of Lipari subsources.

USF #	Area	Li	Na	Mg	Al	Si	P	K	Ca	Sc	Ti	V	Mn	Fe
USF4560	Mt. Guardia	67	18496	149	55817	379466	66	29912	4835	0	380	0	406	8213
USF4565	Mt. Guardia	92	26536	178	67214	360438	41	32140	5476	1	431	0	477	11265
UFS4574	Mt. Guardia	102	24483	176	73286	356706	59	33844	4759	0	468	0	470	9904
USF4590	Mt. Guardia	94	25140	97	67095	361642	58	34469	5744	1	411	0	418	8919
USF4594	Mt. Guardia	64	20967	90	53289	378721	57	33373	4086	0	348	0	366	8325
USF4597	Mt. Guardia	71	17871	83	54560	380494	26	32150	3640	0	332	0	377	8440
USF4600	Mt. Guardia	73	22041	160	63826	369023	80	30913	4681	3	453	0	419	9001
USF4615	Mt. Guardia	68	22596	91	60650	373682	24	28891	4951	0	324	1	381	7612
USF4620	Mt. Guardia	81	23943	349	73965	351471	63	38244	7768	0	528	0	456	10549
USF4638	Mt. Guardia	94	23826	361	72149	348460	154	37918	8451	1	605	0	616	16203
USF4639	Mt. Guardia	60	26893	88	66407	359248	117	38526	4739	0	421	0	431	8906
USF4658	Mt. Guardia	56	18205	123	72745	365708	93	29432	4251	0	364	1	374	7289
USF4688	Canneto Dentro	94	26255	210	68682	359832	68	34991	5467	2	262	0	421	8272
USF4689	Canneto Dentro	78	19364	306	63722	369988	85	30137	5475	2	429	5	443	9862
USF4694	Canneto Dentro	77	18948	162	51370	381511	107	32269	4688	2	355	0	419	8597
USF4696	Canneto Dentro	78	22046	2539	63904	353464	172	29798	8979	1	762	55	739	25157
USF4699	Canneto Dentro	84	23972	219	67427	362853	61	32950	5456	1	507	1	398	9072
USF4702	Canneto Dentro	89	27059	313	72810	354446	81	34915	4604	1	526	3	427	10571
USF4705	Canneto Dentro	92	25435	235	75531	350109	181	39066	5925	2	453	5	448	10169
USF4706	Canneto Dentro	83	26436	390	74112	351912	76	35937	4623	2	428	2	504	12302
USF4710	Canneto Dentro	77	23332	303	65954	365032	340	31676	4615	0	441	2	432	9736
USF4817	Northside Gabellotto Gorge	87	24377	160	70897	359823	51	34181	5227	0	372	0	439	7965
USF4818	Northside Gabellotto Gorge	91	27309	225	65554	362016	65	32353	6197	2	387	1	485	9316
USF4819	Northside Gabellotto Gorge	72	20880	197	60526	371981	36	30210	4869	2	378	0	588	10237
USF4820	Northside Gabellotto Gorge	83	24443	170	69680	359277	70	37256	4629	0	258	0	453	8443
USF4821	Northside Gabellotto Gorge	78	20591	154	74672	354829	780	31173	9126	0	494	0	568	11168
USF4825	Northside Gabellotto Gorge	79	17986	193	73953	363343	72	28760	5511	1	433	0	472	8783
USF4826	Northside Gabellotto Gorge	77	21085	189	57979	376043	139	29691	4997	1	366	1	443	7716
USF4827	Northside Gabellotto Gorge	86	22204	170	74838	356902	91	32452	5089	0	336	0	488	10585
USF4828	Northside Gabellotto Gorge	99	30065	224	64552	356660	50	41830	5192	1	430	0	466	9189
USF5841	Base of Gabellotto Gorge	85	32373	202	68170	350820	72	43171	5245	1	462	0	413	9719
USF5842	Base of Gabellotto Gorge	82	27116	256	59911	363585	39	40010	5015	1	428	1	461	9333
USF5843	Base of Gabellotto Gorge	94	28632	197	63638	358035	54	42402	4705	1	435	1	477	9655
USF5844	Base of Gabellotto Gorge	82	28224	218	59463	364343	86	37430	5315	0	464	0	476	9633
USF5845	Base of Gabellotto Gorge	19	38774	165	77264	339201	101	37247	5343	1	531	0	262	14210
USF5846	Northside Gabellotto Gorge	89	28202	191	57661	365659	67	38997	5095	1	367	0	449	9158
USF5848	Northside Gabellotto Gorge	56	20467	640	49242	381377	135	30964	5392	2	483	7	386	9836
USF5849	Gabellotto Gorge	83	27747	183	59565	366295	58	36426	4369	1	416	1	439	8980
USF5850	Gabellotto Gorge	127	31184	201	72160	346199	52	47419	4871	2	454	0	472	9254

_{continued}**Table 2.** LA-ICP-MS analyses of Lipari subsources.

USF #	Area	Co	Cu	Zn	Rb	Sr	Y	Zr	Nb	Sb	Cs	Ba	La	Ce	Pr	Nd	Sm	Eu	Gd	Tb
USF4560	Mt. Guardia	0	4	28	236	6	37	111	42	1	13	2	30	70	8	33	8	0	6	1
USF4565	Mt. Guardia	0	22	33	304	9	40	131	62	1	13	6	32	73	8	36	7	0	6	1
UFS4574	Mt. Guardia	1	4	29	302	5	49	154	74	1	17	6	46	85	10	39	9	0	8	1
USF4590	Mt. Guardia	0	6	28	276	7	39	111	51	1	15	4	39	77	8	35	8	0	7	1
USF4594	Mt. Guardia	0	3	25	301	4	30	82	43	1	13	4	27	59	6	27	6	0	5	1
USF4597	Mt. Guardia	1	13	19	252	3	37	116	50	1	12	2	27	55	7	25	6	0	5	1
USF4600	Mt. Guardia	0	11	35	289	7	49	122	55	1	13	6	29	66	8	31	8	0	6	1
USF4615	Mt. Guardia	0	6	17	254	4	28	111	40	1	12	4	28	60	6	29	7	0	5	1
USF4620	Mt. Guardia	0	5	34	288	6	38	136	52	1	15	4	36	69	8	34	7	0	7	1
USF4638	Mt. Guardia	0	418	74	285	6	76	157	56	1	14	6	54	106	14	56	15	0	14	2
USF4639	Mt. Guardia	0	353	64	309	5	37	115	53	1	19	5	35	75	8	31	7	0	5	1
USF4658	Mt. Guardia	0	390	50	301	9	30	138	49	1	14	8	34	74	8	32	7	0	5	1
USF4688	Canneto Dentro	0	7	29	306	6	35	130	45	1	16	10	43	95	10	41	8	0	6	1
USF4689	Canneto Dentro	0	11	32	269	18	36	136	63	1	13	21	45	81	8	35	7	0	6	1
USF4694	Canneto Dentro	0	10	28	258	9	26	125	44	1	14	19	45	82	9	37	6	0	6	1
USF4696	Canneto Dentro	5	10	32	255	46	49	155	41	0	12	47	50	93	10	40	9	0	7	1
USF4699	Canneto Dentro	0	4	22	263	10	40	128	49	1	14	16	47	87	9	42	7	0	6	1
USF4702	Canneto Dentro	0	7	33	279	9	30	138	63	1	16	17	46	93	9	37	7	0	5	1
USF4705	Canneto Dentro	0	11	28	254	16	33	146	50	1	16	22	55	102	12	48	9	0	7	1
USF4706	Canneto Dentro	2	13	32	337	18	33	154	48	0	12	18	38	76	8	32	6	0	5	1
USF4710	Canneto Dentro	0	8	38	251	21	37	131	47	1	16	25	46	92	10	42	7	0	5	1
USF4817	Northside Gabellotto Gorge	0	9	21	247	14	36	155	48	1	15	13	66	111	11	44	8	0	8	1
USF4818	Northside Gabellotto Gorge	0	8	32	311	11	35	170	67	1	15	13	54	123	11	50	7	0	6	1
USF4819	Northside Gabellotto Gorge	0	50	23	303	9	43	153	58	1	13	14	60	105	10	47	9	0	7	1
USF4820	Northside Gabellotto Gorge	0	9	35	289	11	36	146	48	1	15	14	53	82	8	35	5	0	4	1
USF4821	Northside Gabellotto Gorge	0	31	37	282	12	57	158	48	1	16	13	82	150	16	65	13	0	11	2
USF4825	Northside Gabellotto Gorge	0	5	50	261	16	40	204	43	0	10	5	46	86	10	38	9	0	7	1
USF4826	Northside Gabellotto Gorge	0	6	23	259	14	30	123	36	1	13	19	85	132	11	53	8	0	6	1
USF4827	Northside Gabellotto Gorge	0	11	41	301	11	42	203	63	1	17	13	57	104	10	44	8	0	7	1
USF4828	Northside Gabellotto Gorge	1	10	54	293	11	28	121	34	1	15	8	38	80	8	37	6	0	5	1
USF5841	Base of Gabellotto Gorge	0	6	47	300	12	33	164	46	1	18	13	46	102	9	41	6	0	6	1
USF5842	Base of Gabellotto Gorge	1	9	51	292	26	29	133	35	1	16	115	39	86	9	38	6	0	5	1
USF5843	Base of Gabellotto Gorge	0	14	68	316	10	27	126	37	1	15	11	39	89	8	37	5	0	6	1
USF5844	Base of Gabellotto Gorge	1	13	57	292	11	27	133	33	1	14	10	40	87	8	37	6	0	5	1
USF5845	Base of Gabellotto Gorge	0	8	26	163	15	37	193	65	1	4	13	41	63	7	34	6	0	7	1
USF5846	Northside Gabellotto Gorge	0	30	61	280	10	28	122	36	1	15	10	38	83	8	37	6	0	6	1
USF5848	Northside Gabellotto Gorge	1	58	52	195	55	24	111	29	1	14	64	38	88	9	41	6	0	5	1
USF5849	Gabellotto Gorge	0	9	53	258	10	29	144	38	1	15	11	41	90	8	40	6	0	7	1
USF5850	Gabellotto Gorge	0	3	47	250	12	35	150	45	1	18	13	46	91	10	46	7	0	7	1

_{continued}**Table 2.** LA-ICP-MS analyses of Lipari subsources.

USF #	Area	Dy	Ho	Er	Tm	Yb	Lu	Hf	Pb	Th	U
USF4560	Mt. Guardia	7	1	4	1	4	1	5	21	37	12
USF4565	Mt. Guardia	5	1	3	0	4	1	5	25	39	15
UFS4574	Mt. Guardia	8	1	4	1	4	1	4	22	40	14
USF4590	Mt. Guardia	7	1	4	1	3	1	4	25	39	13
USF4594	Mt. Guardia	5	1	3	0	3	1	3	27	32	14
USF4597	Mt. Guardia	6	1	4	1	4	1	4	17	28	11
USF4600	Mt. Guardia	6	1	3	1	4	1	5	23	33	12
USF4615	Mt. Guardia	6	1	4	1	3	1	5	23	32	13
USF4620	Mt. Guardia	7	1	4	1	5	1	5	24	40	15
USF4638	Mt. Guardia	14	2	7	1	7	1	7	28	45	13
USF4639	Mt. Guardia	6	1	4	1	4	1	4	34	39	15
USF4658	Mt. Guardia	6	1	4	0	3	0	5	26	39	14
USF4688	Canneto Dentro	7	1	4	0	3	1	5	23	41	17
USF4689	Canneto Dentro	6	1	3	0	4	1	4	21	44	15
USF4694	Canneto Dentro	7	1	4	0	3	0	5	26	48	17
USF4696	Canneto Dentro	7	1	5	1	5	1	5	20	43	13
USF4699	Canneto Dentro	7	1	5	1	3	1	5	18	41	15
USF4702	Canneto Dentro	7	1	4	1	4	1	5	21	43	16
USF4705	Canneto Dentro	7	1	5	1	5	1	5	22	51	17
USF4706	Canneto Dentro	5	1	3	0	3	1	4	20	35	14
USF4710	Canneto Dentro	7	1	4	1	3	1	5	24	43	16
USF4817	Northside Gabellotto Gorge	7	1	4	1	5	1	7	23	50	16
USF4818	Northside Gabellotto Gorge	7	1	3	1	4	1	5	24	49	19
USF4819	Northside Gabellotto Gorge	6	1	4	1	4	1	7	23	54	17
USF4820	Northside Gabellotto Gorge	6	1	3	0	4	1	5	22	38	14
USF4821	Northside Gabellotto Gorge	9	1	5	1	5	1	6	27	52	17
USF4825	Northside Gabellotto Gorge	5	1	5	1	5	1	5	23	55	16
USF4826	Northside Gabellotto Gorge	7	1	4	1	4	1	5	25	42	14
USF4827	Northside Gabellotto Gorge	7	1	4	1	4	1	6	23	50	17
USF4828	Northside Gabellotto Gorge	4	1	3	0	4	1	5	28	44	17
USF5841	Base of Gabellotto Gorge	5	1	3	1	4	1	5	29	44	18
USF5842	Base of Gabellotto Gorge	6	1	4	0	5	1	5	30	45	17
USF5843	Base of Gabellotto Gorge	5	1	3	0	4	1	5	26	40	16
USF5844	Base of Gabellotto Gorge	6	1	4	1	4	1	6	28	45	16
USF5845	Base of Gabellotto Gorge	6	1	4	1	5	1	8	56	44	13
USF5846	Northside Gabellotto Gorge	5	1	3	0	4	0	5	27	44	17
USF5848	Northside Gabellotto Gorge	5	1	3	0	4	0	4	27	42	16
USF5849	Gabellotto Gorge	6	1	3	1	4	1	5	24	46	17
USF5850	Gabellotto Gorge	6	1	4	0	4	1	5	26	45	19

introduced to the torch. A normalization method described by Gratuze et al. (2001) describes the method employed.

About 40 elements were measured using a resolution of 6000. The high resolution was necessary to reduce the number of ions striking the multiplier caused by several of the high concentration elements (Na, Al, Si, K, and Fe). Relative concentrations for all elements were determined by comparing the unknowns to the NIST glass and obsidian standards. To convert the relative concentrations into absolute values, normalization was accomplished converting the relative concentrations to oxides and then normalizing the total to 100%. This method yielded satisfactory concentrations for all major and trace elements.

Analysis by XRF at MURR

Energy-Dispersive X-Ray Fluorescence analysis was performed using a Spectro X-lab 2000 equipped with a Bragg-polarized excitation source. Because plane-polarized photons may not scatter into the plane of polarization, the amount of Compton and coherent scattered radiation seen by a detector when using a Bragg-polarized source in a Cartesian geometry is greatly reduced. For the Spectro X-lab 2000, with a typical degree of polarization of ca. 85%, the scattered radiation background is reduced by a factor of 7 in comparison with direct excitation of the sample. This results in the detection limits and sensitivities improved by factors of 4 for geological samples. The full-width-half-maximum energy resolution of the detector used in these measurements was 135 eV for the 5.90 keV Mn Ka X-ray.

Obsidian samples larger than 1 cm diameter were mounted on the XRF with the most flat surface face downward. The XRF measurements were made using a combination of five excitation targets with a Pd anode: molybdenum for Fe thru Sr and Hf thru Th (35 kV, 4.4 mA), aluminum oxide for Ag thru Nd (52 kV, 5.7 mA), palladium for Y thru Mo (40 kV, 6 mA), cobalt for K thru Mn (30 kV, 1 mA), and highly-oriented pyrolytic graphite for Na thru Cl (15 kV, 13 mA). The method was calibrated with data from 22 pressed-pellets made from geological standard reference materials.

Analysis by pXRF at USF

Analyses by pXRF were conducted with different models of the Bruker Tracer. For all three, the same filter (0.006" Cu, .001" Ti, .012" Al) was used to reduce the background and enhance the precision of the results for X-rays from 17 keV to 40 keV which represent the K-alpha peaks for elements Fe to Mo. Model III-V+ has a Si-Pin detector, resolution approximately 190 eV at 10,000 cps, and the excitation source a Rh target X-ray tube. The Bruker III-SD uses a silicon drift detector (SDD), with count rates greater than 100,000 cps, and thus reduced analysis time necessary. The Bruker V*i* model has an even more sensitive detector, and can be run at 50 kV and 35 μA, expanding the elements that may be detected and with greater sensitivity. All analyses have been conducted using the 8 mm beam size, with geological samples of sufficient width and infinite thickness. Analytical data are calibrated by analyzing with the same instrument a set of 40 obsidian standards produced by MURR based on values obtained from INAA, LA-ICP-MS, and XRF. pXRF analyses were also conducted on geological samples from the historic outcrops.

Table 3. pXRF analyses of Lipari subsources.

USF #	Subsource	Fe	Rb	Sr	Y	Zr	Nb	Fe/Sr	Rb/Sr
4687	Canneto Dentro	12567	280	68	45	157	35	185	4,1
4689	Canneto Dentro	12464	274	67	44	161	33	185	4,1
4690	Canneto Dentro	11466	264	44	38	160	32	258	5,9
4691	Canneto Dentro	12544	266	50	42	158	34	251	5,3
4695	Canneto Dentro	11664	264	46	40	159	36	255	5,8
4697	Canneto Dentro	10380	264	37	37	154	33	278	7,1
4699	Canneto Dentro	13468	270	57	46	162	38	237	4,8
4701	Canneto Dentro	12835	287	45	42	163	36	286	6,4
4702	Canneto Dentro	13038	291	46	46	164	40	286	6,4
4703	Canneto Dentro	11282	273	45	43	165	37	251	6,1
4704	Canneto Dentro	11388	273	47	41	159	34	242	5,8
4705	Canneto Dentro	10472	255	39	41	150	30	270	6,6
4706	Canneto Dentro	11991	270	49	39	158	34	242	5,5
4707	Canneto Dentro	10904	266	37	37	153	33	292	7,1
4708	Canneto Dentro	10735	257	45	42	147	34	239	5,7
4709	Canneto Dentro	11593	272	52	40	156	35	221	5,2
4710	Canneto Dentro	11514	270	47	42	160	33	247	5,8
4711	Canneto Dentro	11587	268	43	37	158	35	268	6,2
4712	Canneto Dentro	11225	260	38	45	151	32	294	6,8
4713	Canneto Dentro	12072	275	50	46	155	36	241	5,5
4714	Canneto Dentro	12029	275	49	42	188	34	245	5,6
6424	Gabellotto	10765	256	17	44	162	35	623	14,8
6426	Gabellotto	11966	279	19	44	182	37	630	14,7
6427	Gabellotto	11304	274	17	47	174	39	671	16,2
6429	Gabellotto	10746	276	19	42	179	35	573	14,7
6433	Gabellotto	10716	281	18	43	166	36	591	15,5
6434	Gabellotto	11228	281	18	40	175	34	629	15,8
6435	Gabellotto	11506	278	18	42	169	36	641	15,5
6436	Gabellotto	11757	287	20	42	184	34	587	14,3
6437	Gabellotto	11524	279	17	43	166	34	661	16,0
6439	Gabellotto	11537	279	19	47	173	37	609	14,7
6443	Gabellotto	9793	269	17	48	166	30	580	16,0
6443	Gabellotto	10664	262	20	43	159	34	533	13,1
28318	Gabellotto	11257	281	21	45	180	33	547	13,7
28319	Gabellotto	11404	289	18	41	177	41	620	15,7
28320	Gabellotto	11097	291	18	38	182	37	627	16,4
28321	Gabellotto	11584	288	18	43	176	37	652	16,2
28322	Gabellotto	11399	267	19	44	174	36	609	14,2
28323	Gabellotto	11619	287	19	41	176	31	598	14,8
28324	Gabellotto	12027	283	19	38	166	36	637	15,0
28325	Gabellotto	11706	301	19	36	175	38	608	15,6
28326	Gabellotto	12884	301	20	50	192	41	642	15,0
28327	Gabellotto	12710	315	17	48	187	38	730	18,1
28329	Gabellotto	13437	310	22	41	195	37	608	14,0
28330	Gabellotto	12730	303	22	45	185	37	582	13,8

Table 3. pXRF analyses of Lipari subsources.

USF #	Subsource	Fe	Rb	Sr	Y	Zr	Nb	Fe/Sr	Rb/Sr
28331	Gabellotto	11080	288	18	44	183	35	623	16,2
28332	Gabellotto	12608	301	19	45	194	42	674	16,1
28333	Gabellotto	10423	248	15	34	160	36	690	16,4
28334	Gabellotto	11226	266	21	44	173	35	534	12,7
28335	Gabellotto	10273	305	17	33	185	29	609	18,1
28336	Gabellotto	11019	263	20	41	169	38	553	13,2
28337	Gabellotto	11438	283	19	37	177	36	615	15,2
28338	Gabellotto	10971	266	18	50	176	32	611	14,8
28339	Gabellotto	11213	273	17	42	184	32	673	16,4
28340	Gabellotto	11433	277	18	43	168	38	653	15,8
28341	Gabellotto	12845	307	26	34	171	35	497	11,9
28342	Gabellotto	11561	280	26	31	178	31	436	10,6
28343	Gabellotto	11004	250	16	43	162	27	688	15,6
28344	Gabellotto	11850	271	19	45	182	32	633	14,5
28345	Gabellotto	13848	341	20	44	194	39	694	17,1
28346	Gabellotto	10554	270	13	40	160	35	812	20,8